CHAPTER 5

CFD STUDY ON RECTANGULAR MINICHANNEL HEAT SINK

This chapter presents the CFD simulation of minichannel heat sink to predict the temperature and velocity profile using hybrid nanofluids. In the available literature, two methods (single-phase and multi-phase) were used to investigate the effect of the suspension of nanoparticles into the base fluid. The first approach is the single-phase model (homogeneous model) in which both the fluid and the particles are in thermal equilibrium and flow at the same local velocity **(Mojarrad et al., 2013 and Tiwari et al., 2014)** while the second approach is the multi-phase model. The multi-phase model is based on the assumption that the phases (i.e., fluid and solid particles) have strong coupling and particles closely travel with the flow **(Lotfi et al., 2010).** In the present investigation, the multi-phase mixture model has been used to examine the performance of minichannel with hybrid nanofluid as a coolant. Al_2O_3-TiO_2, Al_2O_3-SiC and Al_2O_3-Cu dispersed hybrid nanofluids have been considered in the present numerical investigation. The effect of different particle ratios has been presented for Al_2O_3-TiO_2/water hybrid nanofluids.

5.1 Methodology

5.1.1 Two-phase model (multi-phase mixture model)

The mixture model is a simplified multi-phase model that can be used in different ways. The mixture model can model n phases (fluid or particulate) by solving the momentum, continuity, and energy equations for the mixture, the volume fraction equations for the secondary phases, and algebraic expressions for the relative velocities. The mixture model allows to select granular phases and calculates all properties of the

granular phases. This is applicable for liquid-solid flows. The dimensional steady-state governing equations of fluid flow and heat transfer for the two-phase mixture model have been presented **(Lotfi et al., 2010; Labib et al., 2013 and Mojarrad et al., 2013).** The governing equations for the 2 phases (n=2) mixture model can be expressed as:

Continuity equation:

$$\nabla \cdot (\rho_m \vec{V}_m) = 0 \tag{5.1}$$

Momentum equation (Navier- stokes equations):

$$\nabla \cdot (\rho_m \vec{V}_m \vec{V}_m) = -\nabla p_m + \nabla \cdot (\mu_m \nabla \vec{V}_m) + \nabla . \left(\sum_{j=1}^{n} \phi_j \rho_j \vec{V}_{dr,j} \vec{V}_{dr,j} \right) \tag{5.2}$$

Energy equation:

$$\nabla . \sum_{j=1}^{n} (\phi_j \vec{V}_j (\rho_j H_j + p_m)) = \nabla . (k_m \nabla T) \tag{5.3}$$

Volume fraction equation:

$$\nabla \cdot (\phi_p \rho_p \vec{V}_m) = -\nabla \cdot (\phi_p \rho_p \vec{V}_{dr,j}) \tag{5.4}$$

Where mixture velocity, density and viscosity are, respectively,

$$\vec{V}_m = \frac{\sum_{j=1}^{n} \phi_j \rho_j \vec{V}_j}{\rho_m} \tag{5.5}$$

$$\rho_m = \sum_{j=1}^{n} \phi_j \rho_j \tag{5.6}$$

$$\mu_m = \sum_{j=1}^{n} \phi_j \mu_j \tag{5.7}$$

The drift velocity of j_{th} phase, which is nanoparticles in this study,

$$\vec{V}_{dr,j} = \vec{V}_j - \vec{V}_m \tag{5.8}$$

The slip velocity (relative velocity) is defined as the velocity of a secondary phase (nanoparticles) relative to the velocity of the primary phase (base fluid):

$$\vec{V}_{pf} = \vec{V}_p - \vec{V}_f \tag{5.9}$$

The drift velocity is related to the relative velocity as:

$$\vec{V}_{dr,p} = \vec{V}_{pf} - \frac{\sum_{j=1}^{n} \phi_j \rho_j \vec{V}_{jf}}{\rho_m} \tag{5.10}$$

$$\vec{V}_{pf} = \frac{\rho_p d_p^2}{18 \mu_m f_{drag}} \frac{(\rho_{p-} \rho_m)}{\rho_p} \vec{a} \tag{5.11}$$

The drag function is determined by **(Schiller and Naumann, 1935)**

$$_{drag} = \begin{cases} 1 + 0.15 \,\mathrm{Re}_p^{0.687} & \mathrm{Re}_p \le 1000 \\ 0.0183 \,\mathrm{Re}_p & \mathrm{Re}_p > 1000 \end{cases} \tag{5.12}$$

Where $\mathrm{Re}_p = (V_m d_p) / \upsilon_m$ and $\vec{a} = g - (\vec{V}_m \cdot \nabla)\vec{V}_m$

where g is the gravitational acceleration and d_p is the nanoparticle diameter. V_m and υ_m are velocity and kinematic viscosity of the mixture (nanofluid).

5.1.2 Single phase (Homogenous) model

Based on the assumptions provided in section 5.1.3, the dimensional governing equations for steady-state condition (continuity, momentum, and energy) using the single-phase model are as follows:

Continuity equation:

$$\nabla.(\rho_f \vec{V}) = 0 \tag{5.13}$$

Momentum equations:

$$\nabla.(\rho_f \vec{V}\vec{V}) = -\nabla p + \nabla.(\mu_f \nabla \vec{V}) \tag{5.14}$$

Energy equation for fluid:

$$\nabla.(\rho_f \vec{V} c_{p,f} T) = \nabla.(k_f \nabla T) \tag{5.15}$$

Energy equation for the solid wall:

$$0 = \nabla.(k_s \nabla T_s) \tag{5.16}$$

In this work, if a nanofluid is used as the coolant, the thermophysical properties (density ρ_f, heat capacity $c_{p,f}$, dynamic viscosity μ_f, and thermal conductivity k_f) in the governing equations are replaced by those of the hybrid nanofluids, ρ_{nf}, $c_{p,nf}$, μ_{nf}, and k_{nf}, respectively which were given by Eqs. 5.17 to 5.20.

The density of nanofluid or hybrid nanofluid has been calculated from:

$$\rho_{nf} = (1-\phi)\rho_{bf} + \sum_p \phi_p \rho_p \tag{5.17}$$

where, p and bf refer to nanoparticles and base fluid, respectively. For nanofluid, p = 1 and for hybrid nanofluid, p = 2, ϕ is the overall volume concentration of two different types of nanoparticles dispersed in hybrid nanofluid and is calculated as: $\phi = \phi_{p1} + \phi_{p2}$.

Similarly, the specific heat of nanofluid is calculated as,

$$\rho_{nf} c_{p,nf} = (1-\phi)\rho_{bf} c_{p,bf} + \sum_p \phi_p \rho_p c_{p,p} \tag{5.18}$$

The viscosity of the nanofluid or hybrid nanofluid is calculated using the Batchelor relation **(Batchelor, 1976),** which was proposed for nanofluids with a high volumetric concentration in which hydrodynamic interactions and nanoparticle aggregation are important.

$$\mu_{nf} = \left(1 + 2.5\phi + 6.2\phi^2\right)\mu_{bf} \tag{5.19}$$

Thermal conductivity of hybrid nanofluid has been calculated by **(Takabi and Salehi, 2014)**,

$$\frac{k_{nf}}{k_{bf}} = \frac{(1/\phi)\sum_p \phi_p k_p + 2k_{bf} + 2\sum_p \phi_p k_p - 2\phi k_{bf}}{(1/\phi)\sum_p \phi_p k_p + 2k_{bf} - \sum_p \phi_p k_p + \phi k_{bf}} \tag{5.20}$$

5.1.3 Assumption and boundary conditions

For solving the governing equations, a commercial CFD package (ANSYS/Fluent 18.0) was used with the following assumptions:

1. Fluid flow is incompressible, Newtonian and laminar.
2. The steady-state condition is assumed.
3. The same pressure is considered by all the phases (base fluid and nanoparticles).
4. Nanoparticles are spherical and uniform in size and shape.
5. The nanofluid enters the channel with uniform velocity and temperature with the assumption that both the base fluid and particles have the same velocity and temperature.
6. The flow is equally divided into all the channels with no mal-distribution.
7. Fouling free heat transfer surface has been assumed for the investigation.

The governing equations of two approaches have been solved with the following boundary conditions.

- **Inlet condition:** Velocity inlet was specified at the inlet boundary condition with an absolute reference frame and velocity magnitude normal to the boundary. At the minichannel inlet (x=0), the velocity and temperature are considered as, $V_x=0$, $V_y=0$, $V_z=V$, $T=T_{in}=30^oC$.
- **Outlet condition:** Constant gauge pressure was taken as zero Pascal. Constant backflow temperature was specified in the thermal boundary condition.
- **Wall condition:** Stationary wall with no-slip boundary condition is applied on the walls of the channel.
- The constant and uniform heat flux (50 W/cm^2) is applied to the bottom surface and all other surfaces of minichannel heat sink are assumed to be adiabatic (no heat interaction with ambient).

5.2 Geometry and meshing

The development of geometry and the generation of mesh are important and initial steps of the CFD simulation where energy and momentum transfer equations are solved. The heat sink consists of 9 rectangular cross-sectional minichannels. The minichannel heat sink is made of aluminium covered by an adiabatic acrylic plate on top. A schematic of the structure of a rectangular minichannel heat sink is shown in Fig. 5.1. Dotted red line shows the computational domain for the research. It includes one minichannel and half thickness of fins from both sides of minichannel. Minichannel heat sink consists of rectangular-shaped minichannels having a length of 30 mm, a channel width of 1 mm and a channel height of 3 mm. The materials, properties and dimensions of minichannel have been taken same as with the experiment performed in chapter 4. It is supposed to be that all the minichannels are identical in heat transfer and hydrodynamics. Three elements (i.e., fluid, aluminium and acrylic) are here in the present problem. Three interactions between them are fluid-aluminium, fluid-acrylic plate and aluminium-acrylic plate.

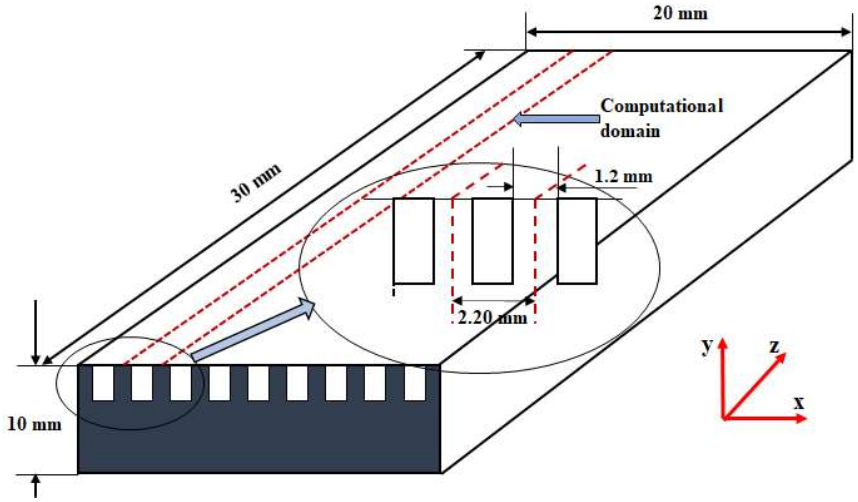

Fig. 5.1 Schematic of minichannel heat sink with computational domain

The hexahedral type grid has been used for the meshing of minichannel heat sink. The purpose of meshing is to reduce the degree of freedom by breakup the computational domains into pieces (grids/elements). Grid generation is the very important part that is directly related to the simulation time and accuracy of the outcomes of study. Thus, dealing with the correct grid generation has same importance as solver operation. Meshing of the computational domain with boundary conditions has been shown in Fig. 5.2.

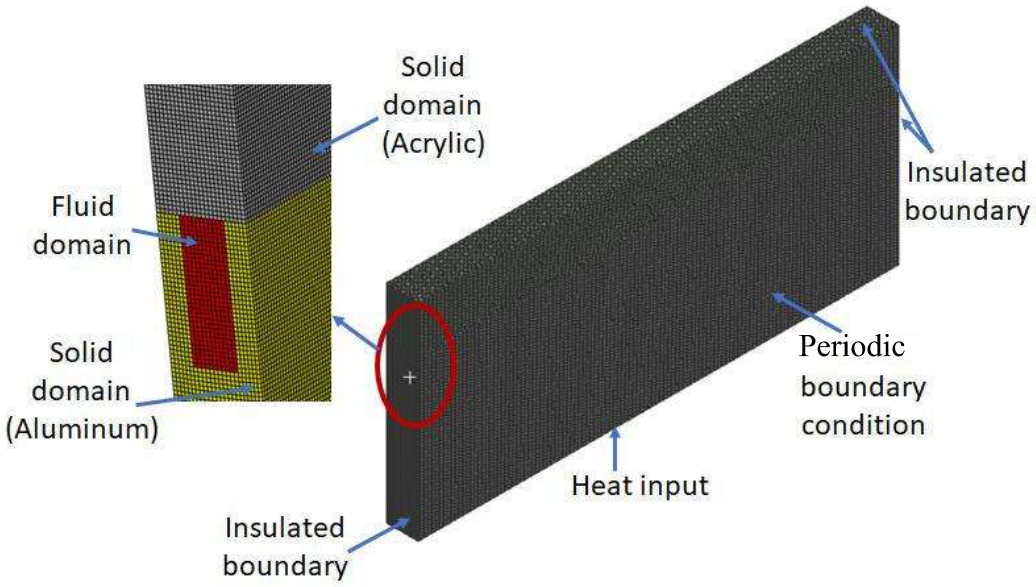

Fig. 5.2 Meshing of computational domain with boundary conditions

5.3 Numerical procedure

The computational fluid dynamics (CFD) calculations are done by using FLUENT (ANSYS 18) that is based on the finite volume method (FVM) discretization. A two-phase mixture model theory is used for simulations. This mixture model is considered for the present study based on the comparison from experimental data. The First order upwind numerical scheme and SIMPLE algorithm are used to discretize the governing equations. The converging criteria are taken as 10^{-6} for all the parameters. A

User Defined Function (UDF) has been prepared and interpreted to calculate the thermophysical properties of the hybrid nanofluids that are not included in the fluent library. UDF includes the correlations that have already been addressed in this chapter's single-phase model section for calculating the different properties. Whereas, properties of the fluid, which is water, are taken from the fluent library.

5.4 Grid independence test

The appropriate quality and quantity of grids are very important in order to ensure the accuracy and time of CFD numerical computation. In this study, the distribution of quadrilateral cells in the computational domain has been determined from tests with a different number of cells for the grid independence test. The grid used have number of elements of 1,840 (coarse), 48,942 (intermediate), 90,768 (fine), 9, 26,250 (very fine) and 1331658. The results of the average heat transfer coefficient and pressure drop for a different number of elements for water in a mini channel of the cross-section area of dimensions 3 mm × 1 mm are presented in **Table 1.** It has been observed that there is very less difference (0.20% in heat transfer coefficient and 2% in pressure drop) in the calculated results after further increasing from grid 9,26,250 to 1331658 grid. As a result, by comparing time usage and accuracy, the very fine grid (926250) has been selected for the simulation.

Table 5.1 Effect of grid size on the heat transfer coefficient and pressure drop

Grid type	**Number of elements**	**Heat transfer Coefficient (W/m^2K)**	**Pressure drop (Pa)**
Coarse	1,840	1002	20.0

Medium	48,942	1949	47.4
Fine	90,768	1956	54.9
Very Fine	9,26,250	1961	58.7
	1331658	1965	60.4

5.5 Validation with the experimental result

The variation of Nusselt number and friction factor (Numerical result) with Reynolds number for Al_2O_3/DI water nanofluid at an inlet temperature of 30°C has been compared with the experimental result in Fig. 5.3 and Fig. 5.4, respectively. Experimental Nusselt number is under predicted and friction factor is over predicted from their numerical results. It is due to assumptions that are considered in the present research. In numerical CFD studies, it is assumed that there is no heat loss but in experiment work there is unavoided heat loss when experiments performed. Also, friction factor is always overpredicted in the experiment because of extra pressure drop due to accuracy and uncertainty in measuring instruments. The average deviations of experimental results from numerical results for Nusselt number using the single-phase model and multi-phase mixture model are 22.57% and 13.21%, respectively. Also, the experimental friction factor is closed to the numerical friction factor predicted by multi-phase mixture model. The average deviations of about 26.1% and 15.13% have been observed for experimental friction factor from numerical results using the single-phase model and multi-phase mixture model, respectively. So, it can be concluded from Fig. 5.3 and 5.4 that multi-phase mixture model gives more accurate results than the single-phase model as similar to previous studies. Thus, further numerical investigation has only been carried out using multi-phase mixture model.

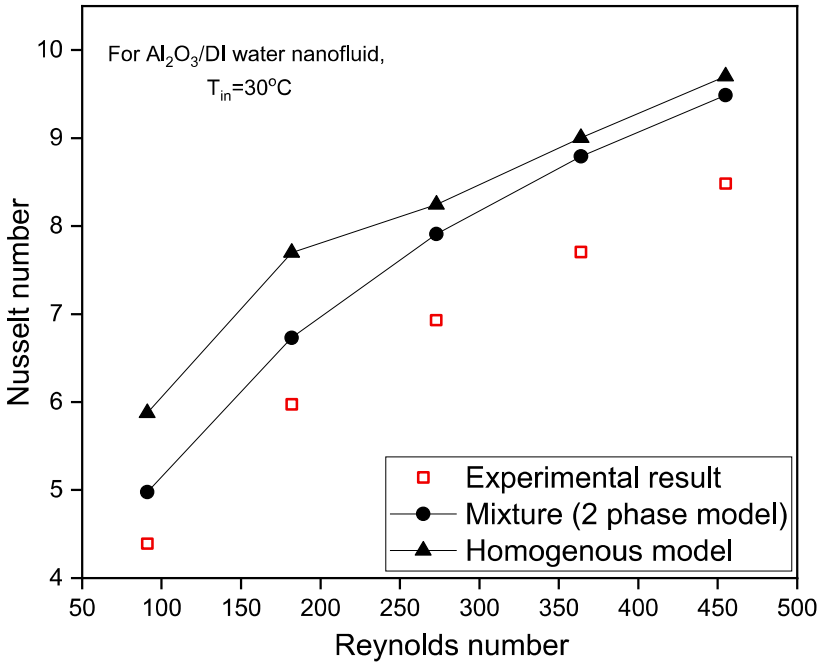

Fig. 5.3 Comparison of numerical result with the experimental result (Nusselt number vs. Reynolds number)

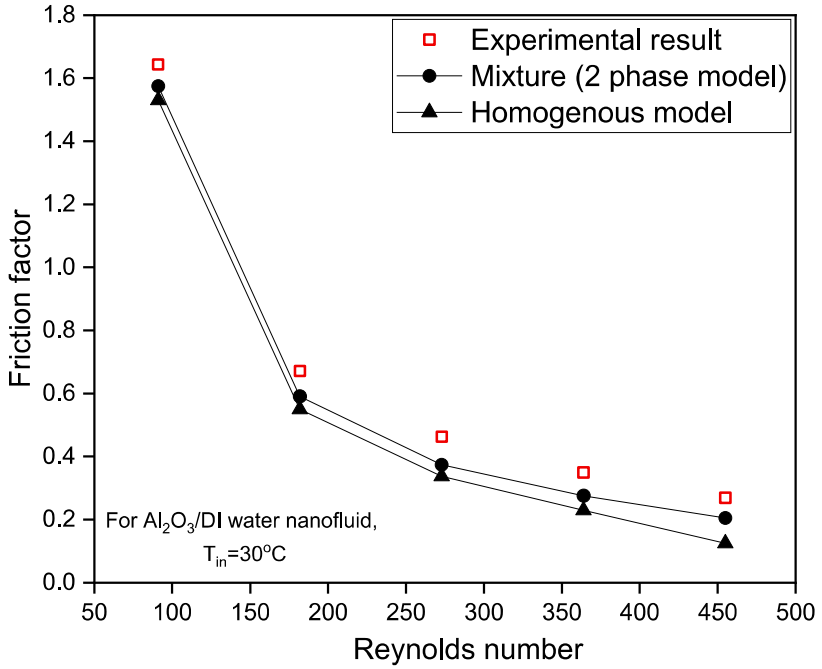

Fig. 5.4 Comparison of numerical result with the experimental result (Friction factor vs. Reynolds number)

5.6 Results and discussion

5.6.1 Comparison of different hybrid nanofluids (0.1 vol%)

DI water, Al_2O_3/water and different hybrid nanofluids have been used in a minichannel heat sink (MCHS). The volume fraction of alumina used in Al_2O_3/water nanofluid is 0.1%. Al_2O_3-TiO_2, Al_2O_3-SiC and Al_2O_3-Cu hybrid nanofluids have been prepared by mixing both nanoparticles in a mixing ratio of 50:50 with the total volume fraction of 0.1%. A rectangular cross-section heat sink was considered for numerical study with the channel dimension of 3 mm × 1 mm and having a length of 30 mm. A constant and uniform heat flux of 50 W/cm^2 has been applied to the bottom surface of minichannel heat sink. The fluid inlet temperature is considered as 30^{o}C.

The variation of surface heat transfer coefficient with flow rate for different working fluids is shown in Fig. 5.5. It can be observed that the heat transfer coefficient increases with an increase in flow rate due to the thinning of the thermal boundary layer. There is found an increment in heat transfer coefficient with the addition of nanoparticles, which may be due to several reasons including an increase in thermal conductivity, different slip mechanisms and the nano-porous and nano-fin effects **(Tiwari et al., 2015).** It is observed from Fig. 5.5 that Al_2O_3+TiO_2 dispersed hybrid nanofluid has less heat transfer coefficient compared to Al_2O_3/water nanofluid. The maximum value of the heat transfer coefficient is 4726.97 W/m^{2}K for Al_2O_3-Cu /DI water hybrid nanofluid. This is mainly due to the high thermal conductivity of copper nanoparticles. Within the studied range, the maximum improvements in the heat transfer coefficient have been observed as nearly 4.2% for Al_2O_3, 3.1% for Al_2O_3-TiO_2, 22.2% for Al_2O_3-SiC and 25% for Al_2O_3-Cu dispersed nanofluids.

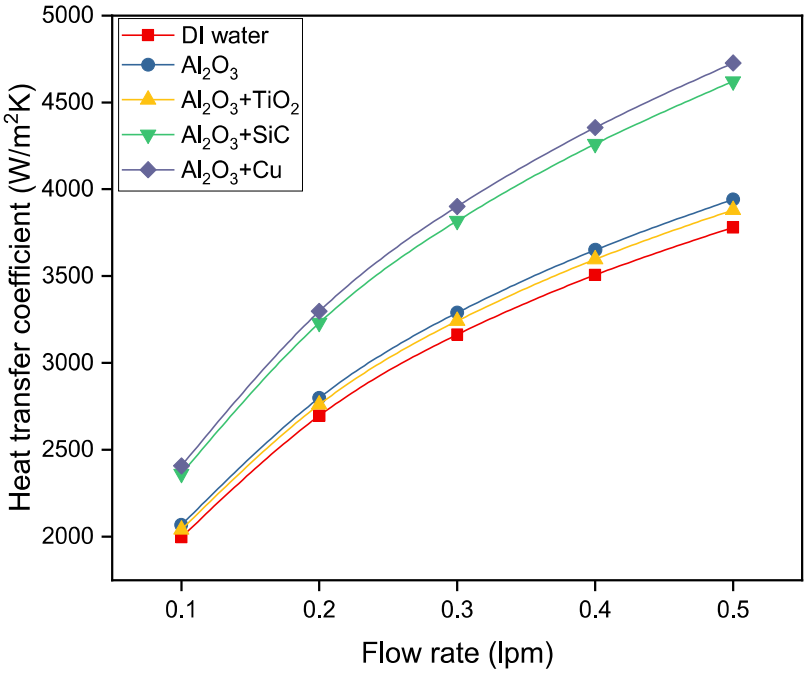

Fig. 5.5 Heat transfer coefficient with flow rate for different working fluids

The variation of Nusselt number with Reynolds number for different working fluids is depicted in Fig. 5.6. It is a well-known fact that the Nusselt number increases with an increase in Reynolds number (as predicted in figures). An increase in Nusselt number can be observed by the addition of nanoparticles and this increase in Nusselt number is due to an increase in heat transfer coefficient as discussed above. Again, Al_2O_3+TiO_2 dispersed hybrid nanofluid has less Nusselt number compared to Al_2O_3/water nanofluid. As shown in figures, the hybrid nanofluid shows very similar behavior with base fluid. The maximum value of the Nusselt number was found for Al_2O_3+Cu about 11.28. Within the studied range and hybrid nanofluids, the maximum improvement in Nusselt number was found as nearly 4.1% for Al_2O_3 nanofluid, 3% for Al_2O_3-TiO_2, 20.9% for Al_2O_3-SiC and 23.52% for Al_2O_3-Cu dispersed hybrid nanofluids.

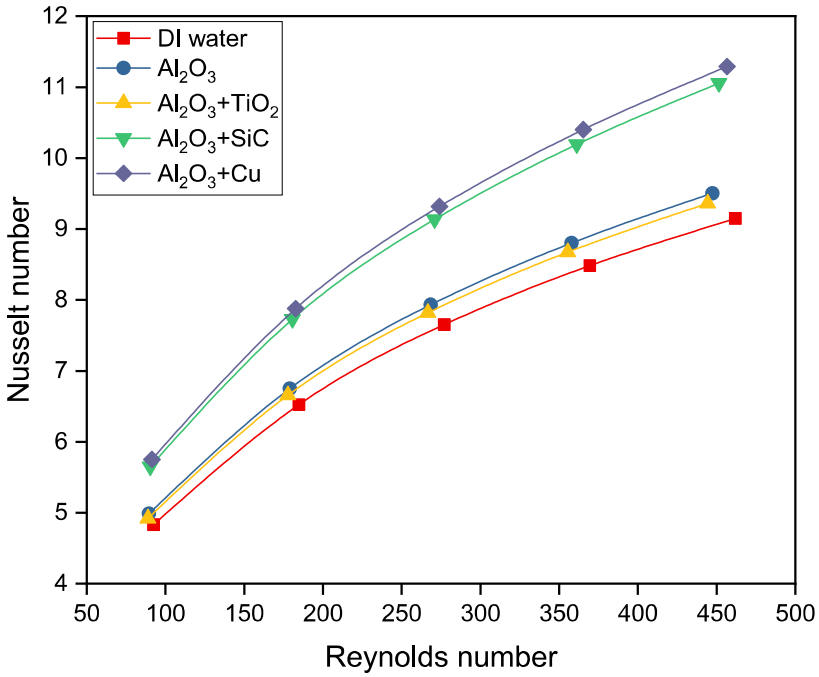

Fig. 5.6 Nusselt number with Reynolds number for different working fluids

The variations of pressure drop with flow rate for different working fluids are shown in Fig. 5.7. Pressure drop is increasing with the rise in flow rate from 0.1 to 0.5 lpm. It can also be observed that the difference in the increase in pressure drop also increases significantly with an increase in flow rate (Reynolds number). It is known that the pressure drops are directly proportional to the mass flux and viscosity, and the mass flow is dominant over the viscosity at the high flow rate (Reynolds number). By the addition of nanoparticles, pressure drop increases due to the dual effect of increasing viscosity and density. The addition of TiO_2 nanoparticles in Al_2O_3 nanofluid does not have a significant effect on pressure drop for the same average particle size due to approximate the same density of both nanoparticles. Al_2O_3-TiO_2 dispersed hybrid nanofluid has the same value for pressure drop as Al_2O_3 nanofluid. A maximum pressure drop has been observed for Al_2O_3-Cu dispersed hybrid nanofluid. A maximum enhancement of 19.1 % has been found for Al_2O_3-Cu/DI water hybrid nanofluid.

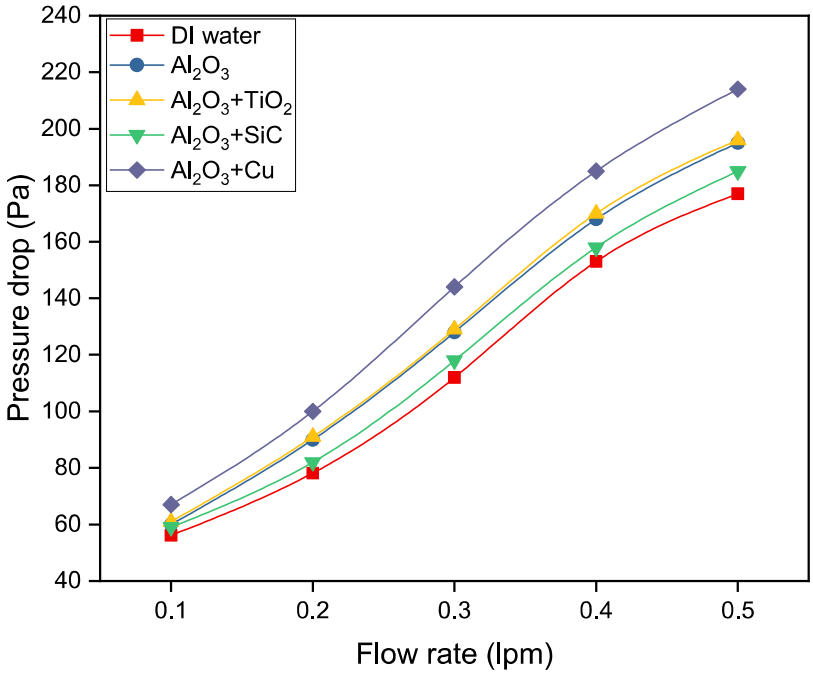

Fig. 5.7 Pressure drop with flow rate for different working fluids

Variation of friction factor with Reynolds number has been shown in Fig. 5.8 for different working fluids. It seems that the friction factor decreases with an increase in the Reynolds number, but there is an increase in friction factor with the addition of nanoparticles. No significant variation is observed in the friction factor for Al_2O_3 nanofluid and Al_2O_3-TiO_2 hybrid nanofluid. The friction factor has its maximum value 1.45 for DI water, 1.56 for Al_2O_3 nanofluid, 1.59 for Al_2O_3-TiO_2, 1.53 for Al_2O_3-SiC and 1.75 for Al_2O_3-Cu dispersed hybrid nanofluid. The decrease in friction factor with Reynolds is due to because of laminar fluid flow in a pipe friction factor is inversely proportional to Reynolds number and the increase in friction factor with the addition of nanoparticles was due to an increase in pressure drop.

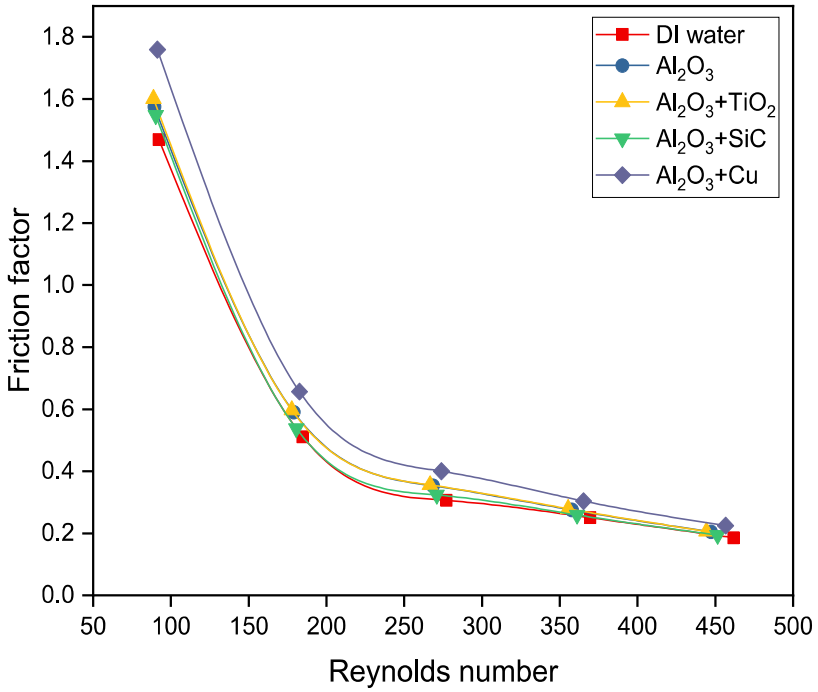

Fig. 5.8 Friction factor with Reynolds number for different working fluids

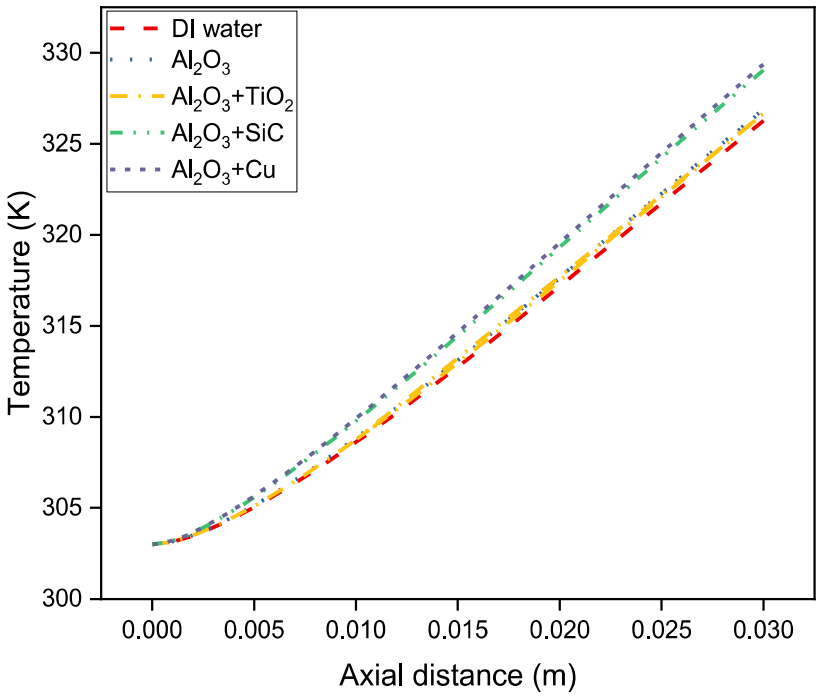

Fig. 5.9 Temperature profile of different working fluids along the length of the channel

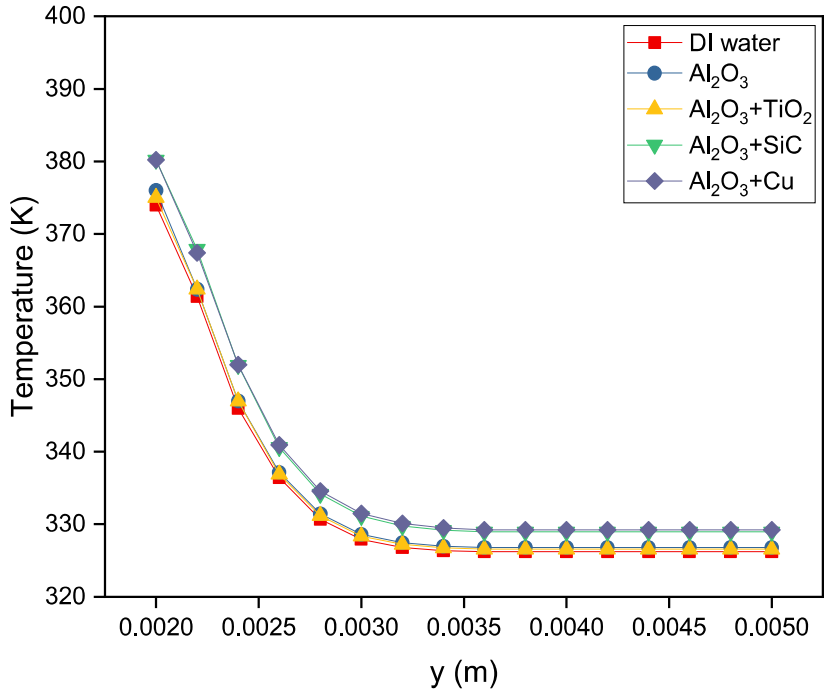

Fig. 5.10 Temperature profile of different working fluids at channel outlet

Figs. 5.9 and 5.10 present the temperature profile of different working fluids as DI water, Al_2O_3 nanofluid, Al_2O_3-TiO_2, Al_2O_3-SiC and Al_2O_3-Cu dispersed hybrid nanofluid along the length of the channel (centreline) and outlet mid-width of the channel in minichannel heat sink, respectively. The outlet temperature is found to increase with the dispersion of nanoparticles. This is due to the decrease in specific heat capacity. Temperature profiles are identical, but due to more heat transfer, nanofluids yield higher temperature values than water at the outlet.

5.6.2 Al_2O_3+TiO_2 hybrid nanofluid (0.1 vol%)

A similar numerical study is done by using Al_2O_3+TiO_2 hybrid nanofluids in different mixing ratios. Minichannel heat sink consists of 9 parallel rectangular-shaped minichannels having a length of 30 mm, a channel width of 1 mm and a channel height

of 3 mm. The constant heat flux (16.67 W/cm^2) is applied to the bottom surface and all other surfaces of minichannel heat sink are assumed to be adiabatic.

The variations of surface heat transfer coefficient with flow rate for different working fluids are shown in Fig. 5.11 at 30°C inlet temperature. It can be observed that the heat transfer coefficient increases with an increase in inlet velocity due to the thinning of the thermal boundary layer. There is found an increment in the heat transfer coefficient with the addition of nanoparticles as compared to base fluid (DI water). The reasons are mentioned in the previous section (i.e., section 5.6.1). As TiO_2 nanoparticle fraction is increasing in the nanofluid, the heat transfer coefficient is decreasing mainly due to the low thermal conductivity of TiO_2 nanoparticles. The maximum value of the heat transfer coefficient is 3937.3 W/m^2 K for Al_2O_3/DI water nanofluid. The maximum improvement in the heat transfer coefficient has been observed as nearly 8.5% for Al_2O_3/DI water nanofluid.

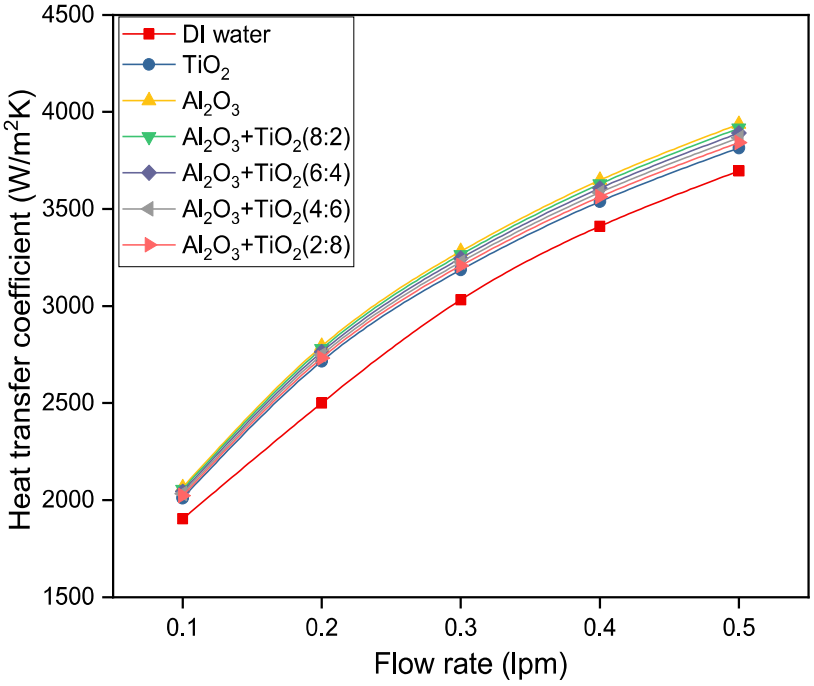

Fig. 5.11 Variation of heat transfer coefficient with flow rate

The variation of Nusselt number with Reynolds number is shown in Fig. 5.12 for different working fluids. Nusselt number increases with flow rate (as predicted figure). An increase in Nusselt number can be observed with the addition of nanoparticles and this increase in Nusselt number is due to an increase in heat transfer coefficient as discussed above. It is shown in figures that the hybrid nanofluid shows very similar behavior with base fluid, although dissimilar to the nanofluids, the Nusselt number for hybrid nanofluids is strongly dependent on the volume ratio of nanoparticles also.

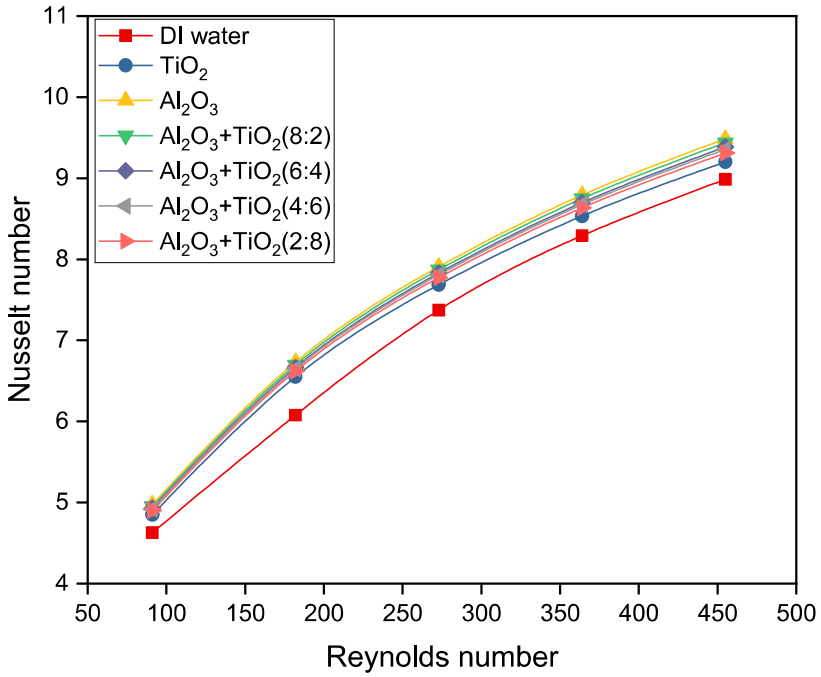

Fig. 5.12 Variation of Nusselt number with Reynolds Number

The variation of pressure drop with flow rate for different working fluids is shown in Fig. 5.13. There is an increment in pressure drop with an increase in flow rate. By the addition of nanoparticles, pressure drop increases due to dual effects of increasing viscosity and density. For all the nanofluids and Al_2O_3-TiO_2 hybrid nanofluids with different nanoparticles fraction (0:10, 2:8, 4:6, 6:4, 8:2 and 10:0), there is no significant

change for pressure drop. The addition of Al_2O_3 nanoparticles in TiO_2 nanofluid does not have a significant effect on pressure drop for the same average particle size. The maximum value of pressure drop is 201.2 N/m^2 for Al_2O_3/DI water nanofluid at 0.5 lpm.

Variation of friction factor with Reynolds number is shown in Fig. 5.14. It seems that the friction factor decreases with an increase in Reynolds number, but there is no significant increment in friction factor with the addition of nanoparticles. The magnifying view of specified area (blue rectangle) is presented in Fig. 5.14. It has been concluded that Al_2O_3 and Al_2O_3+TiO_2 mixtures working fluids are overlapped. The maximum value of the friction factor is 1.73 for Al_2O_3/DI water nanofluid. The decrease in friction factor with Reynolds number (as flow rate increases, Reynolds number increase) is due to because of laminar fluid flow in a pipe friction factor is inversely proportional to Reynolds number.

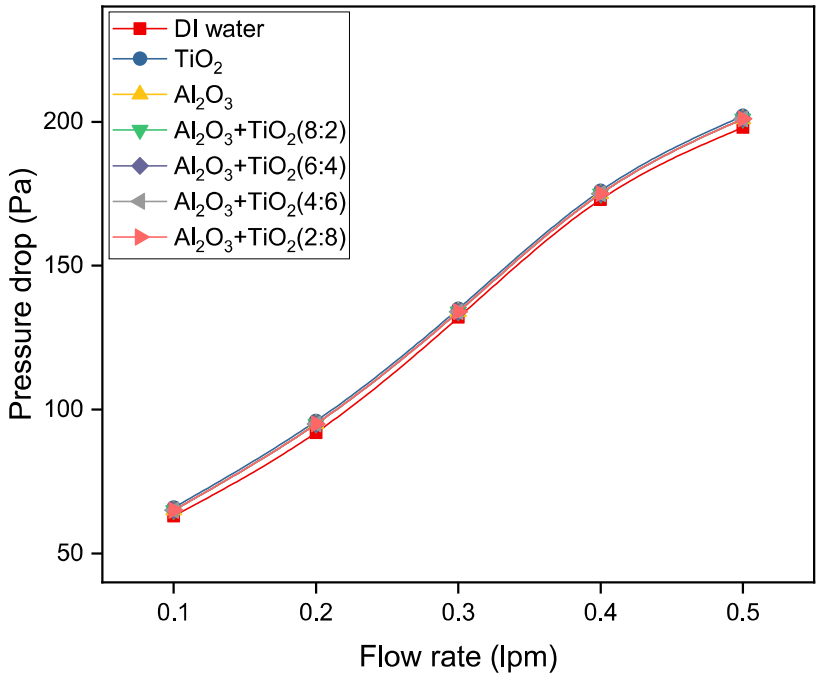

Fig. 5.13 Variation of Pressure drop with the flow rate

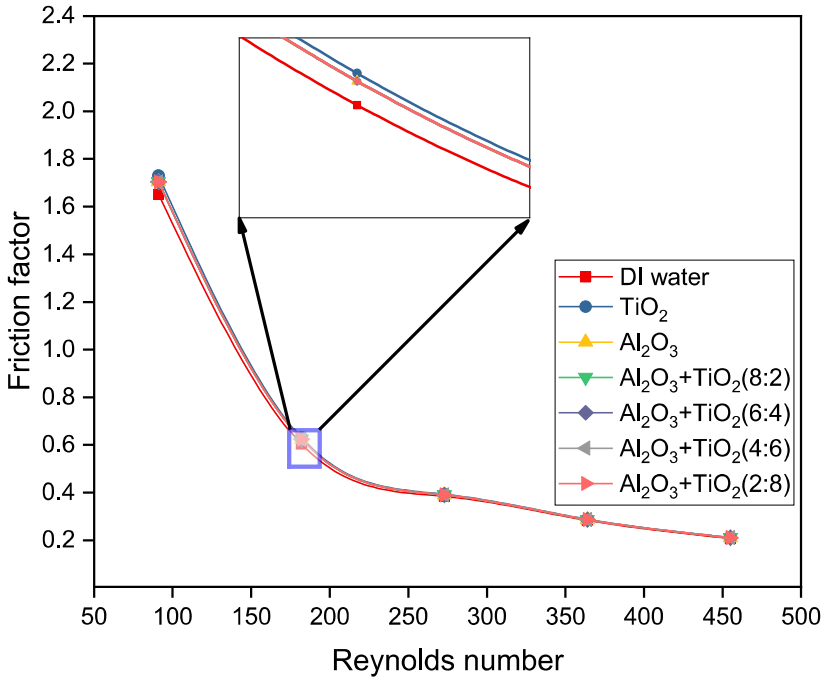

Fig. 5.14 Variation of friction factor with Reynolds Number

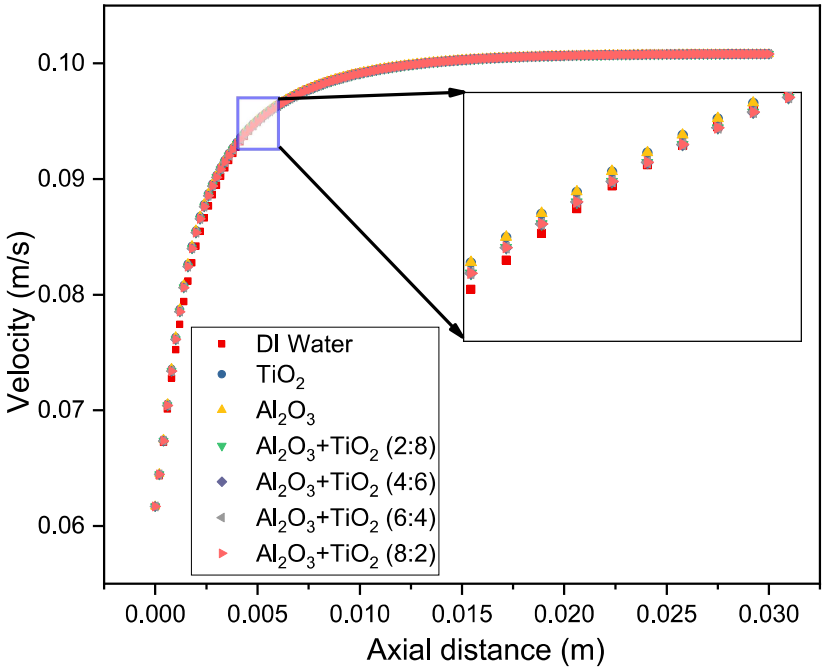

Fig. 5.15 Velocity profile of water and 0.1 vol% nanofluid along the length of the channel

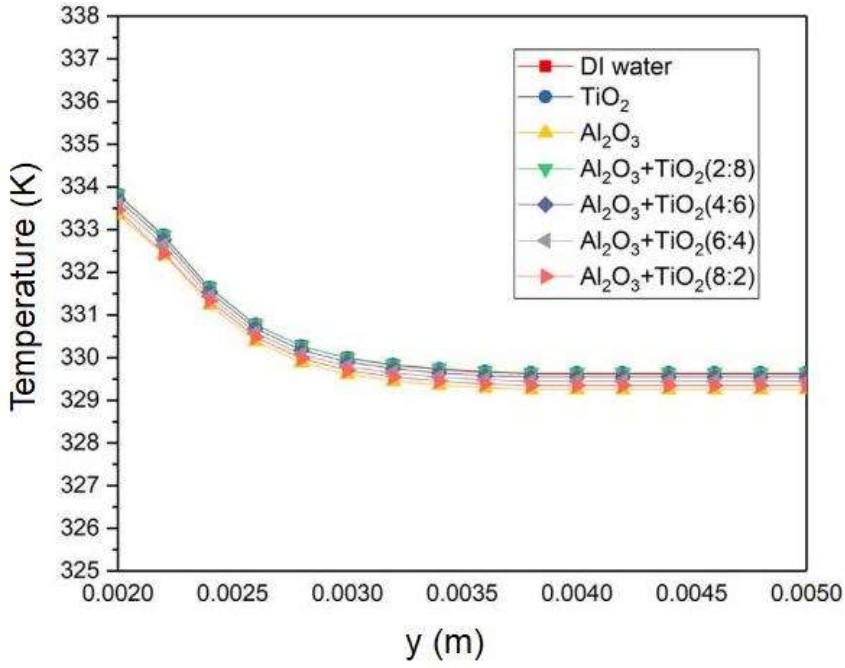

Fig. 5.16 Temperature profile of water and different hybrid nanofluids at channel outlet

Velocity profile of DI water and Al_2O_3-TiO_2 hybrid nanofluid with different particle ratios along the length of the channel (centreline) in minichannel heat sink of having channel height of 3 mm has been shown in Fig 5.15. Blue rectangle presents magnifying view of specified area in Fig. 5.14. It can be seen that there is a decrease in developing and there is a slight increase in the developing length by the addition of hybrid nanoparticles because of the increase in Reynolds number for the same inlet velocity, which thinness the hydrodynamic boundary layer. Fig. 5.14 confirms that flow is fully developed near the outlet. The temperature profile of DI water, Al_2O_3 nanofluid, TiO_2 nanofluid and 0.1vol% Al_2O_3-TiO_2 hybrid nanofluid at outlet mid-width of the channel in minichannel heat sink has been shown in Fig 5.16. Temperature profiles are similar, although, due to more heat transfer, nanofluids yield higher temperature values that water.

5.7 Highlights

- Due to better capture of the heat transfer and flow mechanisms of nanofluids (relative motion between base fluid and nanoparticles), a two-phase mixture model reveals a better agreement with the experimental data for minichannel, in comparison to the single-phase approach.
- The heat transfer coefficient and Nusselt number are higher for hybrid nanofluids having nanoparticles of higher thermal conductivity.
- Pressure drop and friction factor do not show any difference for hybrid nanofluids having approximately the same size and shape. There may be some deviation due to the difference in nanoparticle densities.
- No significant and visible difference in velocity profiles is observed for different hybrid nanofluids due to the same size and shape of nanoparticles.
- Temperature profiles are identical, but hybrid nanofluids yield higher temperature values than base fluid (DI water) at channel outlet due to more heat transfer.
- Hydrodynamic developing length slightly increases with the addition of hybrid nanoparticles in base fluid because of the rupturing of the boundary layer due to slip mechanism and micro-convection.